6-16-2011

Shape and Temperature Dependence of Hot Carrier Relaxation Dynamics in Spherical and Elongated CdSe Quantum Dots

Liangliang Chen
Birck Nanotechnology Center, Purdue University, chen277@purdue.edu

Hua Bao
Birck Nanotechnology Center, Purdue University, hbao@purdue.edu

Taizhi Tan
Birck Nanotechnology Center, Purdue University

Oleg Prezhdo
University of Rochester, oleg.prezhdo@rochester.edu

Xiulin Ruan
Birck Nanotechnology Center, Purdue University, ruan@purdue.edu

THE JOURNAL OF PHYSICAL CHEMISTRY C

ARTICLE

pubs.acs.org/JPCC

Shape and Temperature Dependence of Hot Carrier Relaxation Dynamics in Spherical and Elongated CdSe Quantum Dots

Liangliang Chen,[†] Hua Bao,[†] Taizhi Tan,[†] Oleg V. Prezhdo,*[,‡] and Xiulin Ruan*[,†]

[†]School of Mechanical Engineering and Birck Nanotechnology Center, Purdue University, West Lafayette, Indiana 47907, United States

[‡]Department of Chemistry, University of Rochester, Rochester, New York 14627, United States

ABSTRACT: Time-domain nonadiabatic ab initio simulations are performed to study the phonon-assisted hot electron relaxation dynamics in a CdSe spherical quantum dot (QD) and an elongated quantum dot (EQD) with the same diameter. The band gap is smaller, and the electron and hole states are denser in the EQD than in the QD. Also, the band gap shows a stronger negative temperature dependence in the EQD than in the QD. Higher frequency phonons are excited and scattered with electrons at higher temperatures for both QD and EQD. The electron−phonon coupling is generally stronger in the EQD than in the QD. The hot electron decay rates calculated from nonadiabatic molecular dynamics show a weaker temperature dependence than the T^{-1} trend in both QD and EQD, which is attributed to the thermal expansion effect. Furthermore, the relaxation of hot electrons proceeds faster and shows stronger temperature dependence in the EQD than in the QD. Our work demonstrates that the shape of quantum dots has a strong impact on the electron decay dynamics.

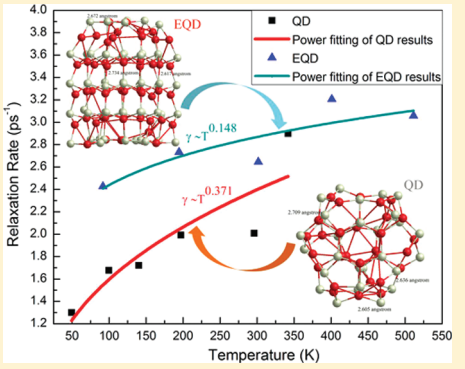

I. INTRODUCTION

Due to the broad bandwidth of the solar spectrum, electrons in semiconductor photovoltaic materials can be excited into different energy levels in the conduction band, and those excited into upper levels are hot electrons. Hot electrons usually quickly lose their excess energy to the lattice via a series of electron−phonon scattering events. To reduce this thermalization loss for possible solar efficiency enhancement, the hot electron relaxation (cooling) rate should be minimized.[1−3] The intrinsic electron−phonon coupling for a bulk material can hardly be modified. However, making the semiconductors into nanostructures such as quantum dots provides possibilities to decouple electrons and phonons. Due to the quantum confinement effect, the electronic structure of quantum dots exhibits discrete energy levels, and the spacing between adjacent levels may become larger than the energy of a single phonon. As a result, hot electrons will need to create multiple phonons simultaneously to relax to lower levels. This higher-order process can result in a lower electron relaxation rate than that of bulk materials.[1,4,5] Slowed hot electron cooling rates have been observed experimentally in quantum dots.[6,7]

Experiments have also shown that both electron−phonon and Auger-type processes can coexist in the electron relaxation process in nanocrystals (NCs).[6] Depending on the types of the materials, status of surface passivation, and types of surface ligands, either the electron−phonon process or the Auger process can dominate the hot carrier relaxation. With a shallow hole trapping surfactant, the Auger process is dominant, and the relaxation is very fast.[6,8−11] However, the Auger process can be avoided if electrons and holes are separated or if electrons and holes have a similar density of states (DOS). Current experimental methods can enable effective separation of electrons and holes, making it possible to decouple the Auger and electron−phonon relaxation processes in NCs.[6,12] For CdSe NCs, with a surfactant of deep hole trapping molecule, such as pyridine, electron−phonon interaction is dominant, and a slow relaxation time of ∼200 ps is observed. This is orders of magnitude longer than that in the bulk system. Slowing down the electron−phonon relaxation is also desired for the possible multiple exciton generation process to be efficient.[3,13−18] Overall, in any situation, slowed electron−phonon coupling is favored for possible solar cell efficiency enhancement.

Due to the fundamental and practical importance of electron−phonon coupling in photovoltaic nanomaterials, it is crucial to understand how the electron−phonon relaxation depends on a variety of factors including material, temperature, nanoparticle size and shape, surface terminations, surfactants, etc.[19] Recently, a nonadiabatic molecular dynamics approach has been developed[20,21] to simulate the hot electron relaxation process in quantum dots,[22−24] and this approach has been used to investigate the temperature dependence of hot carrier relaxation in PbSe quantum dots.[25] It was found that the hot electron relaxation time decreases with increasing temperature, but the dependence deviates from the classical T^{-1} trend due to the thermal expansion effect.[25] On the other hand, no efforts have been devoted yet to investigate the effects of quantum

Received: February 12, 2011
Revised: April 29, 2011
Published: May 19, 2011

dot size and shape on hot electron relaxation, which hinders a fundamental understanding of the structure−property relationship.

In this work, we performed time-domain nonadiabatic molecular dynamics simulations to study the phonon-assisted hot electron relaxation dynamics, in CdSe spherical quantum dot (QD) and elongated quantum dot (EQD). CdSe was chosen as the model material in particular since it is a promising substitute for conventional silicon materials for photovoltaic applications. Aside from bulk CdSe materials, high-crystallinity monodisperse (size distribution ∼10%) CdSe nanocrystals (NCs) have been successfully made using the wet chemistry method,[26,27] and their properties can be tuned by varying the NC size.[28−32] The paper is constructed as follows. A brief review of the NAMD method is first presented. The electronic DOS and band gap are then calculated, from which the optical absorption spectra are derived. The results show clear temperature and shape dependence. The electron−phonon coupling strength spectra are then obtained by taking the Fourier transforms of the time-domain electronic energy levels. The hot electron decay rates are calculated using nonadiabatic molecular dynamics for both QD and EQD, and their dependencies on temperature and shape are analyzed.

II. THEORY AND SIMULATION METHODS

The time-domain nonadiabatic molecular dynamics simulation of the electron−phonon relaxation dynamics is realized by implementing the fewest switching surface hopping (FSSH) technique[20,33,34] in the time-domain Kohn−Sham (TDKS) theory.[35] Details of this method can be found in the ref 24, and here we only outline the procedure.

The electron density is written in the KS representation as[35]

$$\rho(x,t) = \sum_{P=1}^{Ne} |\varphi_P(x,t)|^2 \quad (1)$$

where Ne is the number of electrons and $\varphi_P(x,t)$ are single-electron KS orbitals. Applying the time-dependent variational principle to the expectation value of the KS density functional will lead to the system of coupled equations of motion for the single-particle KS orbitals[35]

$$i\hbar\frac{\partial\varphi_P(x,t)}{\partial t} = H(\varphi(x,t))\varphi_P(x,t),\ P = 1,\ldots,\mathrm{Ne} \quad (2)$$

The time-dependent KS orbitals can be expanded in terms of adiabatic KS orbitals

$$\varphi_P(x,t) = \sum_{K=1}^{Ne} c_{pk}(t)|\tilde{\varphi}_K(x;\mathrm{R})> \quad (3)$$

where R is the ion configuration. After plugging eq 3 into eq 2, the latter transforms into the equation of motion for the expansion coefficients c_{pk}

$$i\hbar\frac{\partial c_{pk}(t)}{\partial t} = \sum_{m=1}^{Ne} c_{pm}(t)(\varepsilon_m\delta_{km} + \mathbf{d_{km}}\cdot\dot{\mathbf{R}}) \quad (4)$$

where $\mathbf{d_{km}}$ is the electron−phonon coupling term defined as

$$\mathbf{d_{km}} = -i\hbar\langle\tilde{\varphi}_k(x;\mathrm{R})|\nabla_R|\tilde{\varphi}_m(x;\mathrm{R})\rangle \quad (5)$$

The nonadiabatic coupling factor is given by[36]

$$\mathrm{NA} = \mathbf{d_{km}}\cdot\dot{\mathbf{R}} = -i\hbar\langle\tilde{\varphi}_k(x;\mathrm{R})|\nabla_R|\tilde{\varphi}_m(x;\mathrm{R})\rangle\cdot\dot{\mathbf{R}} = -i\hbar\left\langle\tilde{\varphi}_k(x;\mathrm{R})\left|\frac{\partial}{\partial t}\right|\tilde{\varphi}_m(x;R)\right\rangle \quad (6)$$

Here, the adiabatic KS orbitals $\tilde{\varphi}_K(x;\mathrm{R})$ are calculated by solving the time-independent KS equations, as implemented[20] in the Vienna Ab initio Simulation Package (VASP).[37] Using FSSH, the probability of a transition from a given state k to another state m within the time interval dt is given by

$$dP_{km} = \frac{b_{km}}{a_{kk}}dt \quad (7)$$

where

$$b_{km} = -2R_e(a_{km}^*\mathbf{d_{km}}\cdot\dot{\mathbf{R}}),\ a_{km} = c_m^*c_k \quad (8)$$

Here, c_m and c_k are the coefficients evolving according to eq 4. As explained in refs 33 and 38, FSSH gives a detailed balance between the upward and downward transitions. From the above equations, the time-dependent electron population in each electronic orbital can be determined. Note that our approach captures the electron−phonon relaxation channel, while the electron−hole interactions are not included.

The geometry optimization, electronic structure calculation, and molecular dynamics (MD) are performed with VASP code using converged plane-wave basis density functional theory (DFT)[37] in simulation cells periodically repeated in three dimensions. Instead of the simultaneous integration of electronic and ionic equations of motion adopted in the Car−Parrinello method, this approach performs an exact evaluation of the instantaneous electronic ground state at each MD step using an efficient Pulay mixing and efficient matrix diagonalization schemes.[37] In our simulations, the initial structures of the $Cd_{33}Se_{33}$ QD and $Cd_{54}Se_{54}$ EQD were generated from bulk wurtzite-structured CdSe (a = 4.3 Å, c = 7.02 Å). Compared with the QD, the EQD is of the same dimension in radial direction but elongated in the axial direction. To prevent spurious interactions between periodic images of the QDs and EQDs, the cells were constructed to have at least 20 Å of vacuum between neighboring QDs and EQDs. The PW91 density functional[39] and Vanderbilt ultrasoft pseudopotentials[40] were used throughout the study. The KS orbitals were expanded using the plane-wave basis set with the energy cutoff of 12.34 Ry (167.9 eV). Higher cutoff energy was also tested, and no significant changes were seen in the resulted configuration and electronic structure. For the CdSe QD and EQD, only Γ point calculations are necessary.

The structure was first fully optimized at 0 K and then heated up different temperatures by MD. Then, a 4 ps microcanonical trajectory was generated at each temperature. The electronic and ionic time steps are set to be 10^{-3} and 1 fs, respectively. The nuclear trajectories from this microcanonical MD were then used to sample 500 initial conditions to create ensemble averages for the nonadiabatic molecular dynamics.

III. RESULTS AND DISCUSSION

A. Geometric Structure and Electronic Density of States.

The initial structures of the QD and EQD were first optimized at 0 K. During the optimization, Cd atoms tend to move inward to minimize the energy, and reconstructions occurred at or near the

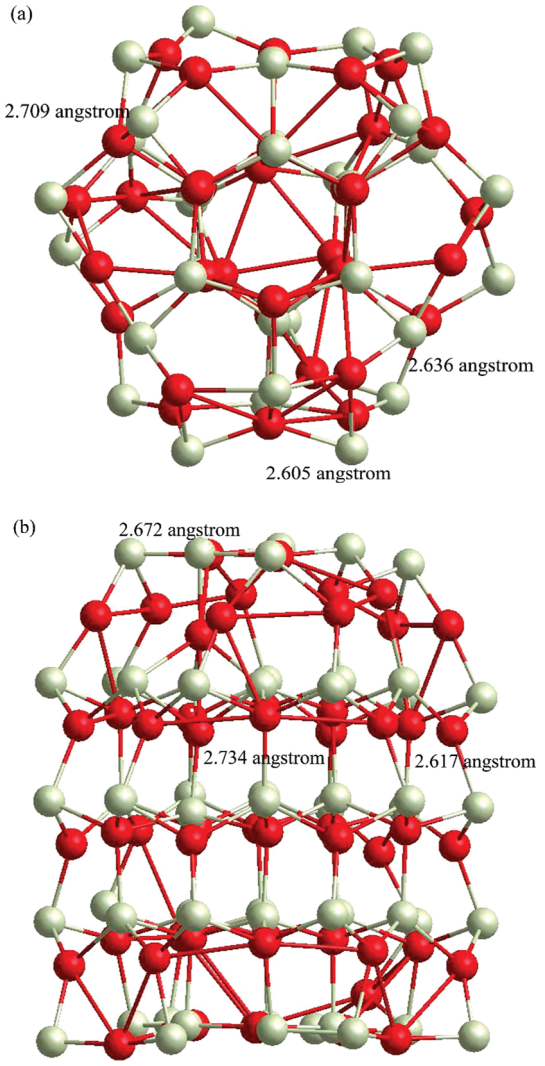

Figure 1. Optimized structures of the $Cd_{33}Se_{33}$ QD (a) and $Cd_{54}Se_{54}$ EQD (b).

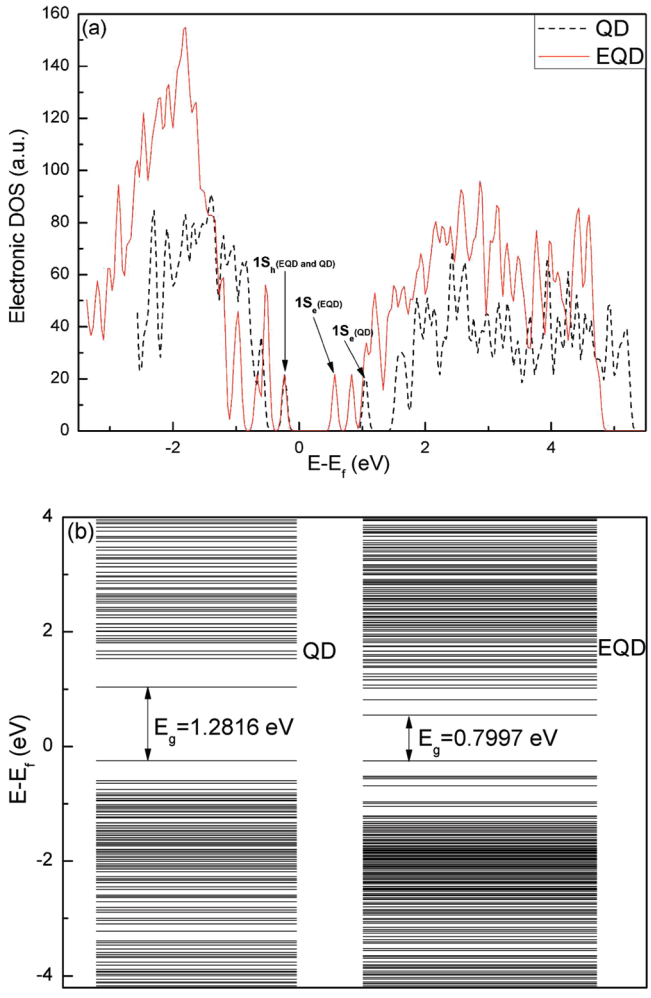

Figure 2. Electronic DOS (a) and structures (b) of the $Cd_{33}Se_{33}$ QD and $Cd_{54}Se_{54}$ EQD.

surface; however, the bulk crystal structures were found to be well preserved in both QD and EQD, as is shown in Figure 1. The optimized QD is∼1.24 nm in diameter, and the optimized EQD is∼1.24 nm in diameter and ∼1.57 nm in length (*c* axis). Some lengths of typical Cd−Se bonds are shown in Figure 1. For the QD, the average Cd−Se bond length is 2.663 Å with a spread between 2.491 and 2.927 Å, while for the EQD, the average Cd−Se bond length is 2.668 Å with a spread between 2.489 and 2.964 Å.

The electronic energy levels and DOS of the CdSe QD and EQD optimized at 0 K are shown in Figure 2. The first peak in the conduction band can be attributed to the 1s electron state ($1S_e$), and the first peak in the valence band is the 1s hole state ($1S_h$). In both cases of QD and EQD, hole states are denser than electron states. This agrees well with the effective mass approximation, in which heavier effective mass is used for holes than electrons ($m_h/m_e \approx 6$).[41] The band gap is estimated by taking the energy difference between the $1S_e$ and $1S_h$ states. The obtained value here is ∼1.3 eV for the QD and ∼0.8 eV for the EQD, both lower than experimental values, which is commonly seen in typical DFT-based simulations.[22−24,42] However, the underpredicted band gap will not significantly affect our calculations of hot electron relaxation since it occurs within the conduction band, and the conduction band curves are expected to be well predicted.

Previous experiments show that the band gap of a CdSe quantum rod whose size is within the strong confinement regime decreases as its length increases.[43] In our case, the EQD and QD together can be viewed as quantum rods with the same diameter but different lengths. The diameter (∼1.24 nm) of both is much smaller than their exciton Bohr radius (∼5.6 nm for bulk CdSe), and therefore the NCs are within the strong quantum confinement regime. This fact can explain why in our simulation the shorter quantum rod, i.e., QD, shows a noticeably wider band gap than the longer quantum rod, i.e., EQD, shown in Figure 2.

The absorption spectra for the CdSe QD and EQD were calculated by summing over individual transitions across the electronic band gap,[25] and the results are shown in Figure 3. According to the DOS, the $1S_e-1S_h$, $1S_e-1P_h$ ($1P_e-1S_h$), and $1P_e-1P_h$ electronic transitions correspond to the absorption maxima at around 1.25, 1.85, and 2.35 eV for the QD and 0.75, 1.2, and 1.7 eV for the EQD. Compared with the QD, the absorption peaks in the EQD occur at lower energies, which is consistent with the fact that the electronic energy levels in the EQD are denser than in the QD. At higher temperatures, the

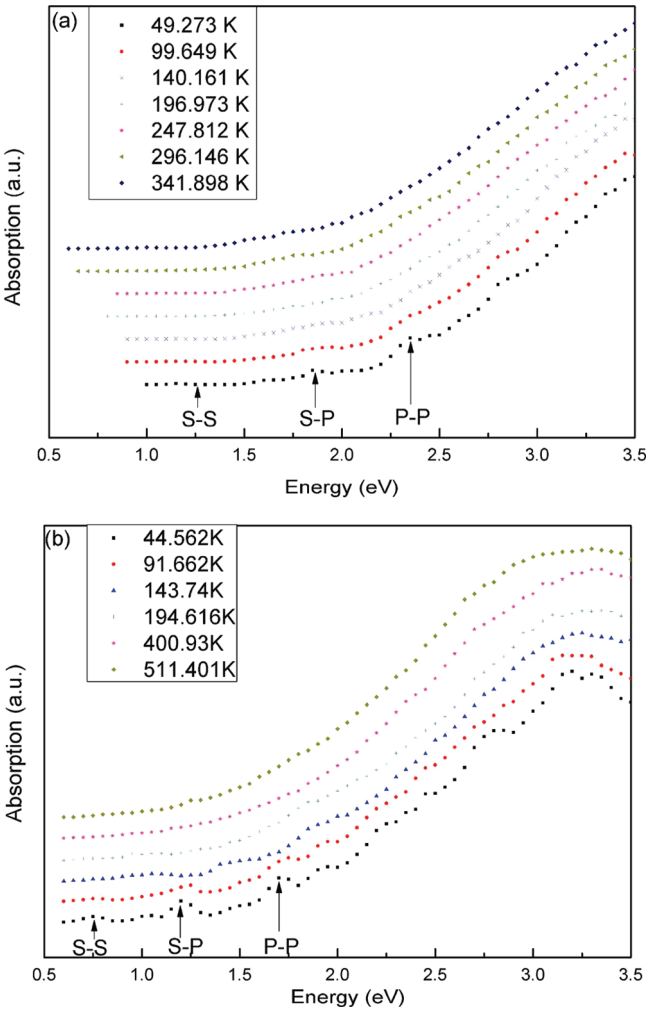

Figure 3. Absorption spectra of the CdSe QD (a) and EQD (b).

absorption peaks are broadened because more phonons are generated and coupled to the photon absorption process. In addition, as temperature increases, the absorption peaks shift to the red side, indicating that the energy band gap probably should have a negative temperature dependence for both QD and EQD.

The temperature dependence of the band gap of the CdSe QD and EQD is shown in Figure 4. These band gap values were calculated by averaging the energy differences between the lowest unoccupied molecular orbitals (LUMO) and highest occupied molecular orbitals (HOMO) over the MD trajectory at the specified temperature. The result can be fitted linearly with slopes of −0.2521 and −0.3824 meV/K for the QD and EQD, respectively. The negative temperature dependence of the band gap for both QD and EQD agrees well with the experiments.[44−46] It is also noticed that the band gap of the smaller quantum dot (QD) shows a weaker temperature dependence than that of the larger quantum dot (EQD), and a similar trend was also observed in experiments by other researchers.[47,48] Proposed by Olkhovet et al.,[47] the temperature dependence of the NC band gap is determined by four factors: dilation of the lattice, thermal expansion of the envelope function, mechanical strain, and electron−phonon coupling, among which electron−phonon coupling makes the most dominant contribution. The electron−phonon coupling consists of intraband and interband coupling. The

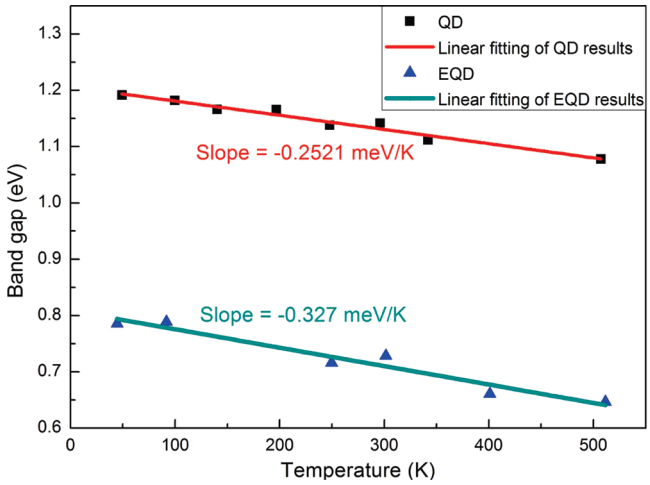

Figure 4. Band gap as a function of temperature for the CdSe QD and EQD.

intraband coupling leads to a negative temperature dependence, while the interband part gives a positive dependence. Since the intraband energy differences for CdSe NCs do not approach the energy gap of bulk CdSe, the intraband coupling contributions are much larger than the interband contributions, and therefore the overall temperature dependence of the band gap is negative.[47] Furthermore, in CdSe NCs, the temperature dependence of ΔE contributed by the intraband part can be approximately related to the electron−phonon coupling strength S, $\Delta E/\Delta T \sim -S$.[47] According to our calculation, which will be shown later in Figure 9, the intraband electron−phonon coupling is slightly stronger in the CdSe EQD than the CdSe QD, which can qualitatively explain the slightly stronger temperature dependence of the band gap in the EQD.

B. Electron−Phonon Coupling. In MD, temperature is evaluated based on the kinetic energy average over the MD trajectory. The time evolutions of the LUMO in both QD and EQD at low and high temperatures are shown in Figure 5. The energy fluctuations are more significant at high temperature than low temperature for both QD and EQD. The LUMO values for the QD and EQD at various temperatures were obtained by averaging the LUMO values over the MD trajectory (4000 fs). As temperature increases, the average LUMO value decreases, which in turn causes the band gap value to decrease.

The phonon modes that can effectively couple to electron relaxation were investigated by taking the Fourier transforms of the time-dependent LUMO energies. The coupling strength spectra at different temperatures are plotted as a function of phonon frequencies in Figure 6. As seen, temperature affects the electron−phonon coupling in two ways. First, at higher temperatures, the coupling spectra are broadened, indicating that more phonon modes are excited and coupled to electrons, which can be attributed to a stronger anharmonic effect at higher temperatures. Second, at higher temperatures, high-frequency tails show up in the spectra, indicating that higher-frequency phonons are excited and coupled to hot electrons. Furthermore, spectral densities are larger, and more high-frequency vibrational modes are involved for the EQD than for the QD, indicating stronger phonon−electron nonadiabatic coupling in the CdSe EQD.

C. Nonadiabatic Relaxation Dynamics of Photoexcited Electrons. In this part, electrons were first excited to initial energy states at ∼0.75 eV above the LUMO and then were

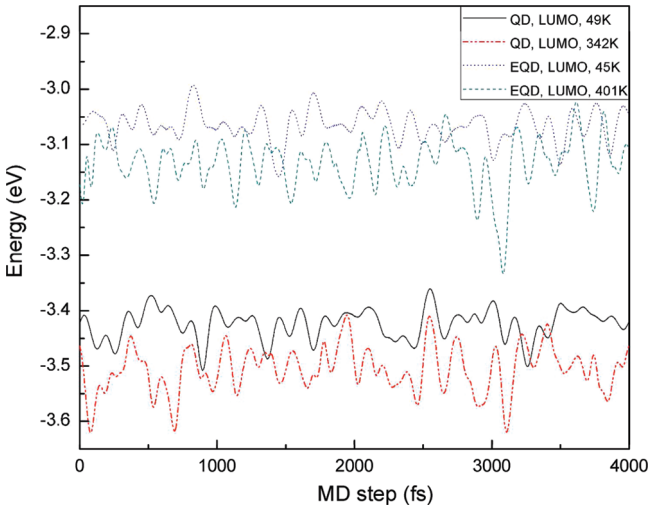

Figure 5. Time evolution of the LUMOs for the CdSe QD and EQD at high and low temperatures.

allowed to relax from the nonequilibrium states to the LUMO. The driving force is electron density perturbation induced by lattice vibrations. Within this energy range, only transitions with the largest optical activities were chosen as the initial conditions. The result of the time-dependent relaxation is shown in Figure 7. For each temperature, a 3.5 ps decay trajectory is plotted, and the zero energy is set at the corresponding average LUMO value. A typical decay curve is composed of two parts, including a short-period Gaussian and thereafter an exponential component, similar to the previous result.[22] In the CdSe QD, electron energies will decay back to zero at the end of the 3.5 ps trajectories when temperature is higher than 50 K. At 342 K, electron energies can sometimes even fall below zero, which can be rationalized by taking into account the significant energy fluctuation at high temperatures. In the case of EQD, most electrons relax back to the LUMO at the end of the trajectories for a wide range of temperatures. The temperature-dependent hot electron decay rate can be easily calculated. In both QD and EQD, hot electrons decay faster at higher temperatures.

To gain a deeper understanding of the underlying relaxation mechanism, the decay rates at different temperatures were extracted from the decay curves, as shown in Figure 8. The decay time here is defined as the time that electrons need to decay to the energy equal to 1/e of their initial energy, and the decay rate is defined as the inverse of the decay time with a unit of ps^{-1}. It can be seen in Figure 8 that hot electrons generally decay faster in the EQD than the QD. As mentioned in Section III.B, the stronger electron−phonon coupling leads to the higher relaxation rate for hot electrons in the EQD. Phonon-assisted electron relaxation can occur via both slow multiphonon and fast resonant-energy-phonon processes, depending on the DOS.[24] In Figure 2, the electron DOS in the QD is different from that in the EQD in two ways. First, the 1S electron state in the QD is well separated from the rest of the CB, while the 1S electron state in the EQD has some overlap with the rest of the CB. Second, in the region well above the LUMO, electron states are denser in the EQD than in the QD. The nonadiabatic coupling defined in eq 6 can be rewritten as

$$\mathrm{NA} = -i\hbar\frac{\langle\tilde{\varphi}_k|\nabla_R H|\tilde{\varphi}_m\rangle}{E_m - E_k}\cdot\dot{\mathbf{R}} \qquad (9)$$

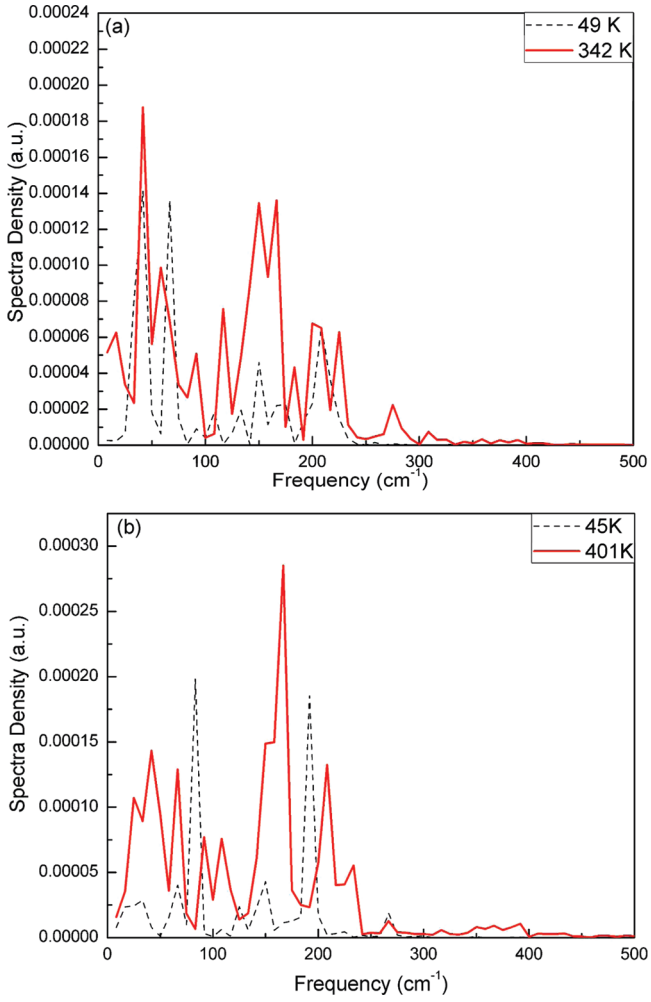

Figure 6. Fourier transforms of the LUMO vibrations for the CdSe QD (a) and EQD (b) at high and low temperatures.

According to Fermi's Golden Rule, the decay rate is proportional to $|\mathrm{NA}|^2$ and thus inversely proportional to the square of the energy difference between transition states, which is $(E_m - E_k)$ in eq 9. Giving the denser energy states in the EQD, the nonadiabatic coupling should be stronger in the EQD, and thus the hot electron relaxation rate should be higher in the EQD.

On the basis of the theoretical model proposed in our previous work,[25] the temperature dependence of the hot carrier relaxation rate could be simply written as

$$\gamma \sim |\mathrm{NA}|^2 \sim |\mathbf{d_{km}}|^2|\dot{\mathbf{R}}|^2 \sim |\mathbf{d_{km}}|^2 T_{MD} \qquad (10)$$

where γ, NA, $\mathbf{d_{km}}$, $\dot{\mathbf{R}}$, and T_{MD} represent the relaxation rate, nonadiabatic coupling, electron−phonon coupling term, ion velocity, and temperature, respectively. The last proportion is based on the statistical thermodynamic definition of temperature. Equation 10 indicates that γ should be proportional to T_{MD} if $|\mathbf{d_{km}}|$ is temperature-independent. However, our calculated results, shown in Figure 8, deviate significantly from the expected trend. The decay rate can be better fitted to $T^{0.371}$ and $T^{0.148}$ for the QD and EQD, respectively. This deviation indicates that $|\mathbf{d_{km}}|$ must be temperature-dependent. To confirm that, we obtained the $|\mathbf{d_{km}}|^2$ defined in eq 5 associated with the initial state and LUMO for both QD and EQD at different temperatures, and the results are plotted in

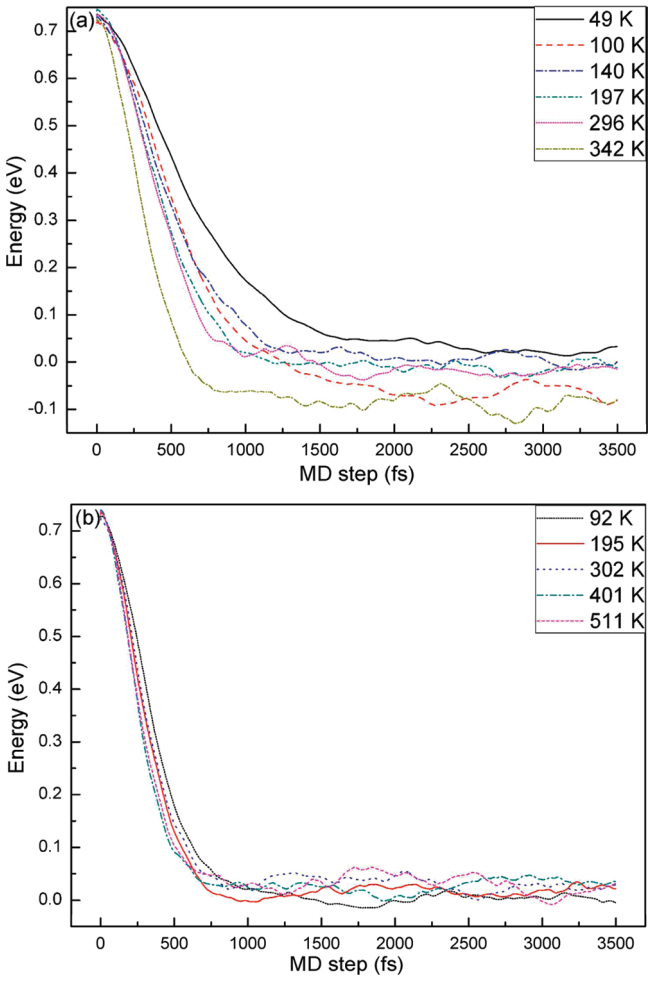

Figure 7. Average electron energy decay at different temperatures for the CdSe QD (a) and EQD (b).

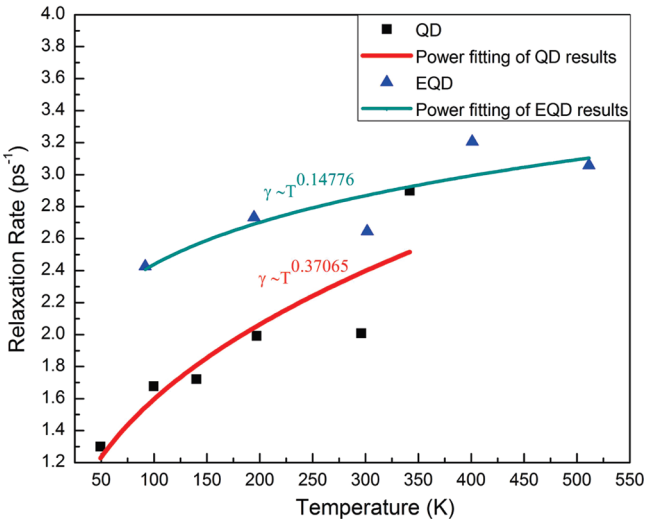

Figure 8. Hot electron relaxation rate as a function of temperature for the CdSe QD and EQD.

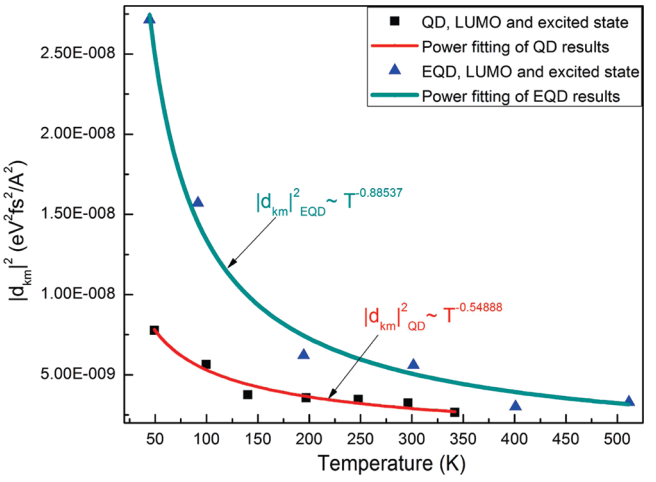

Figure 9. Temperature dependence of $|\mathbf{d}_{km}|^2$ for the CdSe QD and EQD.

Figure 9. It is clear that $|\mathbf{d}_{km}|^2$ does have a negative temperature dependence, which can be fitted to $T^{-0.549}$ and $T^{-0.885}$ for the QD and EQD, respectively. After substituting $|\mathbf{d}_{km}|^2$ with the fitting functions into eq 10, the obtained relationships between γ and T are $\gamma \sim T_{MD}^{0.45}$ for the QD and $\gamma \sim T_{MD}^{0.11}$ for the EQD, which agree well with the previous results from the fitting. Thus, the weaker temperature dependence of the hot electron decay rate can be attributed to the negative temperature dependence of $|\mathbf{d}_{km}|$, which probably arises from the negative dependence of $|\mathbf{d}_{km}|$ on the thermal expansion in NCs.[19] Furthermore, $|\mathbf{d}_{km}|$ has a stronger negative temperature dependence in the EQD than the QD. Experimental results show tha,t for CdSe NCs, as size decreases the lattice constants decrease correspondingly.[49] It could be deduced that lattice parameters in the EQD are larger than those in the QD, and our calculated results shown in Figure 1 confirm that the Cd−Se bond is longer in the EQD than QD. Therefore, assuming the EQD and QD have the same thermal expansion coefficient, a larger thermal expansion is expected in the EQD with the same temperature rise, which will in turn make it reasonable that $|\mathbf{d}_{km}|$ has a stronger negative temperature dependence in the EQD.

IV. SUMMARY

We have used the time-domain DFT and NAMD to study the phonon-assisted hot electron relaxation dynamics in the CdSe QD and EQD. The electronic DOS shows shape-dependent features. The band gap is narrower, and electron and hole states are denser in the EQD than in the QD. The band gap shows negative temperature dependence for both QD and EQD. The temperature dependence is stronger for EQD. By taking the Fourier transforms of the LUMO energies, the electron−phonon coupling spectra were also evaluated. At higher temperatures, higher-frequency phonon modes are induced to scatter with electrons for both QD and EQD. The electron−phonon coupling is stronger in the EQD than in the QD, which favors a generally faster relaxation in the EQD. The hot electron decay rate shows a weaker temperature dependence than expected for both QD and EQD. This could be attributed to the negative temperature dependence of the electron−phonon coupling term $|\mathbf{d}_{km}|$. The hot electron decay rate is higher and shows a stronger temperature dependence in the EQD than in the QD. In all, our work shows that the shapes of NCs can affect the optical and electronic properties of the NCs through modifications of their electronic structure. The results presented in this paper can help

to understand the fundamental mechanisms of hot electron relaxation dynamics in NCs and to guide future experiments.

AUTHOR INFORMATION

Corresponding Author
*E-mail: oleg.prezhdo@rochester.edu; ruan@purdue.edu.

ACKNOWLEDGMENT

This work was partially supported by the National Science Foundation (grant no. CTS-0933559). OVP acknowledges the NSF grant CHE-1050405 for supporting the methods development and DOE grant DE-FG02-05ER15755 for supporting the applied studies.

REFERENCES

(1) Nozik, A. J. *Annu. Rev. Phys. Chem.* **2001**, *52*, 193.
(2) Nelson, J. *The Physics of Solar Cells*; Imperial College Press: London, 2003.
(3) Prezhdo, O. V. *Chem. Phys. Lett.* **2008**, *460*, 1.
(4) Urayama, J.; Norris, T. B.; Singh, J.; Bhattacharya, P. *Phys. Rev. Lett.* **2001**, *86*, 4930.
(5) Yoffe, A. D. *Adv. Phys.* **2001**, *50*, 1.
(6) Guyot-Sionnest, P.; Shim, M.; Matranga, C.; Hines, M. *Phys. Rev. B* **1999**, *60*, R2181.
(7) Pandey, A.; Guyot-Sionnest, P. *Science* **2008**, *322*, 929.
(8) Schaller, R. D.; Pietryga, J. M.; Goupalov, S. V.; Petruska, M. A.; Ivanov, S. A.; Klimov, V. I. *Phys. Rev. Lett.* **2005**, *95*, 196401.
(9) Cooney, R. R.; Sewall, S. L.; Anderson, K. E. H.; Dias, E. A.; Kambhampati, P. *Phys. Rev. Lett.* **2007**, *98*, 177403.
(10) Hendry, E.; Koeberg, M.; Wang, F.; Zhang, H.; Donega, C. D.; Vanmaekelbergh, D.; Bonn, M. *Phys. Rev. Lett.* **2006**, *96*, 4.
(11) An, J. M.; Califano, M.; Franceschetti, A.; Zunger, A. *J. Chem. Phys.* **2008**, *128*, 7.
(12) Guyot-Sionnest, P.; Wehrenberg, B.; Yu, D. *J. Chem. Phys.* **2005**, *123*, 074709.
(13) Schaller, R. D.; Klimov, V. I. *Phys. Rev. Lett.* **2004**, *92*, 186601.
(14) Nozik, A. J. *Nano Lett.* **2010**, *10*, 2735.
(15) Nozik, A. J.; Beard, M. C.; Luther, J. M.; Law, M.; Ellingson, R. J.; Johnson, J. C. *Chem. Rev.* **2010**, *110*, 6873.
(16) Rabani, E.; Baer, R. *Nano Lett.* **2008**, *8*, 4488.
(17) Ellingson, R. J.; Beard, M. C.; Johnson, J. C.; Yu, P. R.; Micic, O. I.; Nozik, A. J.; Shabaev, A.; Efros, A. L. *Nano Lett.* **2005**, *5*, 865.
(18) Witzel, W. M.; Shabaev, A.; Hellberg, C. S.; Jacobs, V. L.; Efros, A. L. *Phys. Rev. Lett.* **2010**, *105*, 137401.
(19) Prezhdo, O. V. *Acc. Chem. Res.* **2009**, *42*, 2005.
(20) Craig, C. F.; Duncan, W. R.; Prezhdo, O. V. *Phys. Rev. Lett.* **2005**, *95*, 163001.
(21) Fischer, S. A.; H., B. F.; Madrid, A. B.; Duncan, W. R.; Prezhdo, O. V. *J. Chem. Phys.* **2011**, *134*, 024102.
(22) Kilina, S. V.; Craig, C. F.; Kilin, D. S.; Prezhdo, O. V. *J. Phys. Chem. C* **2007**, *111*, 4871.
(23) Hyeon-Deuk, K.; Madrid, A. B.; Prezhdo, O. V. *Dalton Trans.* **2009**, 10069.
(24) Kilina, S. V.; Kilin, D. S.; Prezhdo, O. V. *ACS Nano* **2009**, *3*, 93.
(25) Bao, H.; Habenicht, B. F.; Prezhdo, O. V.; Ruan, X. L. *Phys. Rev. B* **2009**, *79*, 235306.
(26) Murray, C. B.; Norris, D. J.; Bawendi, M. G. *J. Am. Chem. Soc.* **1993**, *115*, 8706.
(27) Steigerwald, M. L.; Alivisatos, A. P.; Gibson, J. M.; Harris, T. D.; Kortan, R.; Muller, A. J.; Thayer, A. M.; Duncan, T. M.; Douglass, D. C.; Brus, L. E. *J. Am. Chem. Soc.* **1988**, *110*, 3046.
(28) Halperin, W. P. *Rev. Mod. Phys.* **1986**, *58*, 533.
(29) Wang, Y.; Herron, N. *J. Phys. Chem.* **1991**, *95*, 525.
(30) Satoh, N.; Nakashima, T.; Kamikura, K.; Yamamoto, K. *Nat. Nano* **2008**, *3*, 106.
(31) Efros, A. L.; Efros, A. L.; Poluprovodn, F. T. *Sov. Phys.: Semicond.* **1982**, *16*, 772.
(32) Bussian, D. A.; Crooker, S. A.; Yin, M.; Brynda, M.; Efros, A. L.; Klimov, V. I. *Nat. Mater.* **2009**, *8*, 35.
(33) Duncan, W. R.; Craig, C. F.; Prezhdo, O. V. *J. Am. Chem. Soc.* **2007**, *129*, 8528.
(34) Tully, J. C. *J. Chem. Phys.* **1990**, *93*, 1061.
(35) Marques, M. A. L.; Gross, E. K. U. *Annu. Rev. Phys. Chem.* **2004**, *55*, 427.
(36) Hammes-Schiffer, S.; Tully, J. C. *J. Chem. Phys.* **1994**, *101*, 4657.
(37) Kresse, G.; Furthmuller, J. *Comput. Mater. Sci.* **1996**, *6*, 15.
(38) Parandekar, P. V.; Tully, J. C. *J. Chem. Phys.* **2005**, *122*, 094102.
(39) Perdew, J. P.; Wang, Y. *Phys. Rev. B* **1992**, *45*, 13244.
(40) Vanderbilt, D. *Phys. Rev. B* **1990**, *41*, 7892.
(41) Klimov, V. I.; McBranch, D. W. *Phys. Rev. Lett.* **1998**, *80*, 4028.
(42) Pulci, O.; Onida, G.; Del Sole, R.; Reining, L. *Phys. Rev. Lett.* **1998**, *81*, 5374.
(43) Li, L. S.; Hu, J. T.; Yang, W. D.; Alivisatos, A. P. *Nano Lett.* **2001**, *1*, 349.
(44) Joshi, A.; Narsingi, K. Y.; Manasreh, M. O.; Davis, E. A.; Weaver, B. D. *Appl. Phys. Lett.* **2006**, *89*, 131907.
(45) Kim, C. K.; Lautenschlager, P.; Cardona, M. *Solid State Commun.* **1986**, *59*, 797.
(46) Hang, Z.; Yan, D.; Pollak, F. H.; Pettit, G. D.; Woodall, J. M. *Phys. Rev. B* **1991**, *44*, 10546.
(47) Olkhovets, A.; Hsu, R. C.; Lipovskii, A.; Wise, F. W. *Phys. Rev. Lett.* **1998**, *81*, 3539.
(48) Wise, F. W. *Acc. Chem. Res.* **2000**, *33*, 773.
(49) Neeleshwar, S.; Chen, C. L.; Tsai, C. B.; Chen, Y. Y.; Chen, C. C.; Shyu, S. G.; Seehra, M. S. *Phys. Rev. B* **2005**, *71*, 201307.